NGC 2401: A template of the Norma-Cygnus Arm's young population in the Third Galactic Quadrant

G. Baume[1,2], A. Moitinho[3], R.A. Vázquez[1], G. Solivella[1], G. Carraro[2,4,5] and S. Villanova[2] ⋆

[1] *Facultad de Ciencias Astronómicas y Geofísicas de la UNLP, IALP-CONICET, Paseo del Bosque s/n, La Plata, Argentina*
[2] *Dipartimento di Astronomia, Università di Padova, Vicolo Osservatorio 2, I-35122 Padova, Italy*
[3] *CAAUL, Observatório Astronómico de Lisboa, Tapada da Ajuda, 1349-018 Lisboa, Portugal*
[4] *Astronomy Department, Yale University, P.O. Box 208101, New Haven, CT 06520-8101 USA*
[5] *Departamento de Astronomía, Universidad de Chile, Casilla 36-D, Santiago, Chile*

ABSTRACT

Based on a deep optical CCD ($UBV(RI)_C$) photometric survey and on the Two-Micron All-Sky-Survey (2MASS) data we derived the main parameters of the open cluster NGC 2401. We found this cluster is placed at 6.3 ± 0.5 kpc ($V_O - M_V = 14.0 \pm 0.2$) from the Sun and is 25 Myr old, what allows us to identify NGC 2401 as a member of the young population belonging to the innermost side of the extension of the Norma-Cygnus spiral–arm in the Third Galactic Quadrant. A spectroscopic study of the emission star LSS 440 that lies in the cluster area revealed it is a B0Ve star; however, we could not confirm it is a cluster member. We also constructed the cluster luminosity function (LF) down to $V \sim 22$ and the cluster initial mass function (IMF) for all stars with masses above $M \sim 1 - 2M_{\odot}$. It was found that the slope of the cluster IMF is $x \approx 1.8 \pm 0.2$. The presence of a probable PMS star population associated to the cluster is weakly revealed.

Key words: Galaxy: open clusters and associations: individual: NGC 2401 - Galaxy: structure - Stars: imaging - Stars: Be - Stars: luminosity function, mass function - Individual: LSS 440

1 INTRODUCTION

The open cluster NGC 2401 (=OCL 588 = C0727-138) is an almost unstudied compact grouping of faint stars, but for identification and eye estimates of its angular size and richness. According to the Lyngå (1987) classification, this object is a Trumpler class II 3 p with about 2′ in diameter, which is the same diameter listed in Dias et al. (2002). A recent photometric study on this area carried out by Sujatha et al. (2004) yielded an intriguing result where a relatively far cluster (located at a distance of about 3.1 kpc) shows only a color excess $E_{B-V} = 0$. This fact alone deserves our total attention. Moreover, since NGC 2401 is placed in the Puppis region ($l = 229.67°$; $b = +1.85°$) in the poorly studied Third Quadrant of the Galaxy, the determination of its basic parameters will contribute, together with other cluster studies in the region, to describe more precisely the spiral structure and the star formation history in this part of the Galaxy. This region contains several distant clusters through which information on the kinematics and evolutionary status of the stellar population in the outermost parts of the galactic disk can be obtained. In fact, since the detection of the Canis Major over-density (see p.e. Martin et al. 2004, Momany et al. 2004 for more details), there is a growing interest to get a better description of the stellar population in this region of the Galaxy.

Preliminary results of NGC 2401 can be found in a CCD $UBVRI$ photometric database by Moitinho (2001, 2002) containing brief information for 30 open clusters in the galactic longitude range $217° < l < 260°$. Also recently, Giorgi et al. (2002, 2005), Carraro & Munari (2004), Baume et al. (2004), Carraro et al. (2005a) and Moitinho et al. (2005) published studies of a series of largely overlooked open clusters in the same galactic region.

In this paper we present a detailed study of the membership, reddening, distance and age of NGC 2401. They were derived together with the Luminosity and Initial Mass Functions, two distributions which are fundamental tools for understanding the star formation mechanisms and related astrophysical problems. We also present the first spectrum

⋆ Based on observations collected at CTIO and ESO and CASLEO; Data is only available in electronic form at the CDS via anonymous ftp to `cdsarc.u-strasbg.fr (130.79.128.5)` or via `http://cdsweb.u-strasbg.fr/cgi-bin/qcat?J/A+A//`;
email:gbaume@fcaglp.unlp.edu.ar(GB)

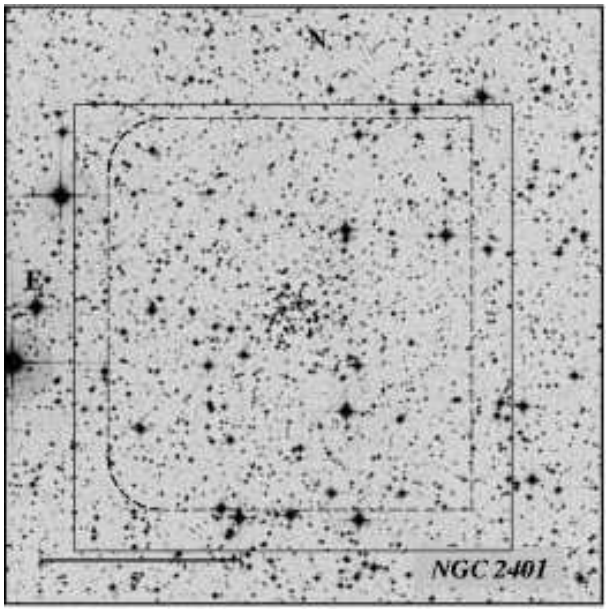

Figure 1. Second generation Digitized Sky Survey (DSS-2), red filter image of the field of NGC 2401. The areas covered by the CTIO and ESO observations are indicated by solid and dashed lines, respectively.

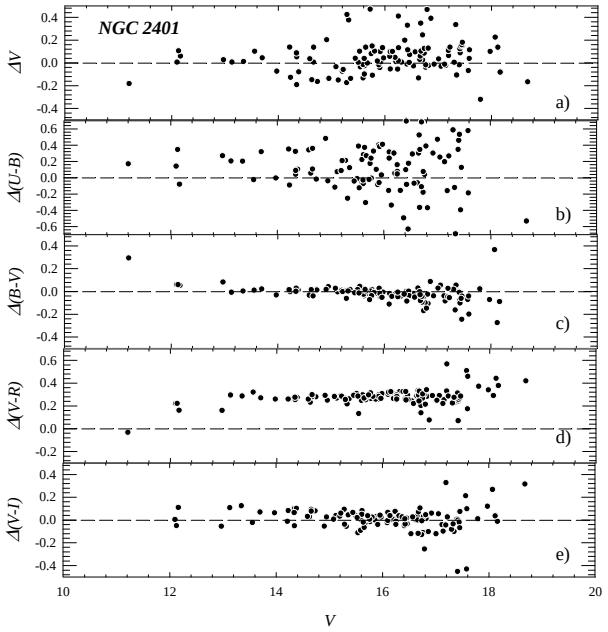

Figure 2. Comparison of our photometry with Sujatha et al. (2004) in the sense "Our data - Their data" (115 stars). Mean differences and their standard deviations (sd) were: $\Delta V = +0.05 \pm 0.14(sd)$; $\Delta(B-V) = -0.02 \pm 0.10(sd)$; $\Delta(U-B) = +0.06 \pm 0.39(sd)$; $\Delta(V-R) = +0.28 \pm 0.07(sd)$ and $\Delta(V-I) = +0.00 \pm 0.11(sd)$

analysis of the peculiar emission star LSS 440 located in the cluster field and try to clarify the possible connection of both objects.

In the next section we introduce the observational material. Sect. 3 is aimed at analyzing the photometric diagrams and to determine memberships. In Section 4 we discuss the LSS 440 main properties; in Sect. 5 we construct and discuss both, the LF and IMF. In Section 6 we studied the possible presence of pre-main sequence (PMS) stars and, finally, in Sects. 7 and 8 we discuss the main findings of this investigation and present the conclusions respectively.

2 DATA SET

2.1 Optical photometric data

CCD $UBV(RI)_C$ images of NGC 2401 were acquired with the CTIO 0.9m telescope during an observing run in January 1998. Observations, reductions, error analysis, and comparison with other photometries were thoroughly described in Moitinho (2001). Additionally, further CCD $V(I)_C$ images were obtained for this object at ESO - La Silla - with the EMMI camera mounted on NTT in the night of December 9, 2002. Typical seeing was about $1''$. The camera has a mosaic of two 2048×4096 pixels CCDs which samples a $9'.9 \times 9'.1$ field. The images were binned 2×2, resulting a scale of $0''.332$/pix. Details on the reductions of these kind of data were given in Baume et al. (2004). The fields covered by CTIO and ESO observations are shown in Fig 1.

Combining both data sets required a detailed comparison of their plate scales and photometric scales. While matching the X,Y pixel coordinates from both sets, we noticed that no one-to-one correspondence could be satisfactorily achieved through a simple linear transformation. Indeed, the residuals of the transformation displayed a jump in the middle of the NTT X axis. This is likely due to the junction between the two CCDs that compose the EMMI camera. Once taking this effect into account, the NTT coordinates were transformed without trouble to the system of the CTIO X-Y positions, and sources from both sets were cross-identified. The RMS residuals of the transformations were around 0.15 CTIO pixels (1 CTIO pixel $\approx 0''.39$). The NTT VI measurements were then tied to the CTIO photometry through linear transformations of the form $V_{CTIO} - V_{NTT} = \alpha_0 + \alpha_1(V-I)_{NTT}$; $(V-I)_{CTIO} = \beta_0 + \beta_1(V-I)_{NTT}$, using stars with estimated errors less than 0.015 mag, which essentially corresponds $V_{CTIO} < 18$mag. The rms of the photometric transformations were ≈ 0.02 mag. Both photometries were then combined by averaging the measurements weighted by their errors. The errors in the CTIO magnitudes are described in Moitinho (2001), and are taken to be the dispersion of the measurements when repeated observations were available, or the errors output by ALLSTAR in the case of single measurements. For the NTT magnitudes the adopted errors were those given by ALLSTAR.

We also cross correlated our data with the ones given by Sujatha et al. (2004) to compare both photometric sets. Figure 2 shows a relatively good agreement in the mean values for V magnitudes and $B-V$ and $V-I$ colors, though the V magnitude spread is quite significant. In addition, there is a noticeable shift between both data sources when $U-B$ and $V-R$ colors are compared. In particular, the spread in $U-B$ is simply huge. These differences could be explained by the different spatial resolution of each observation set

(some crowded areas in Sujatha et al. data were resolved by us), zero point differences in their $U-B$ and $V-R$ measures probably caused by poor atmospheric conditions in the Sujatha et al. observing run and the rather poor quality of their U filter. This way, the strange color excess value $E_{B-V}=0$ computed by them can be explained. It is worth mentioning that our data produce coherent fitting solutions over all the photometric diagrams (see in advance Sect. 3 and Fig. 7). On the other hand, our photometric data are based on a more general and homogeneous data set (Moitinho 2001), which are in agreement to previous studies (when the comparison was possible). Therefore, we can conclude our data are right at all.

2.2 Spectroscopic data

Spectral data for the star LSS 440 ($\alpha_{2000}=07:29:30.1$; $\delta_{2000}=-13:59:13$) were obtained at the 215-cm telescope of CASLEO (Argentina) during the nights of December 6, 7 and 9, 2004. Observations were carried out with a REOSC-DS Cassegrain spectrograph equipped with a Tek 1024×1024 detector. The grating was successively centered at $7^\circ\ 15'$, $8^\circ\ 30'$ and $11^\circ\ 30'$ (on different nights) to get a full spectral range coverage from 3400 Å to 6750 Å in wavelength. The dispersion was 2.5 Å/pixel (resolution ≈ 1800). Two 30 minutes exposure time spectra were taken in each grating position to remove undesirable events such as cosmic rays and to improve the signal–noise ratio of the final spectrum. Comparison lamp (HeNeAr) spectra were acquired between each pair of exposures. Spectra were reduced using IRAF† routines like IMRED, CCDPROC, TWODSPEC and ONEDSPEC using the typical procedure.

2.3 Infrared data and astrometry

Available catalogues, such as 2MASS, are of fundamental importance to perform a more complete analysis of any sky region. Using the CCD X–Y positions of our data we computed their equatorial coordinates. First of all, a matched list of X–Y and RA, DEC was built by visually identifying about 20-30 TYCHO-2 (Høg et al. 2000) and 2MASS stars in each cluster field. The stars in the list were used to obtain transformation equations to get equatorial coordinates for all our measured stars. In a second step we use a computer routine to cross-identify all our sources in common with the same catalogues by matching the equatorial coordinates to the catalogued ones. The rms of the residuals were $\sim 0\farcs15$, which is about the astrometric precision of the 2MASS catalogue ($\sim 0\farcs12$), as expected since most of the coordinates were retrieved from this catalogue.

This procedure allowed to build a photometric $UBVRIJHK$ catalogue that constitutes the main observational database used in this study. Table 1 includes our X–Y positions (in arcseconds, see Fig. 5), equatorial coordinates (epoch 2000.0), optical and infrared photometry. This table is only available electronically.

† IRAF is distributed by NOAO, which are operated by AURA under cooperative agreement with the NSF.

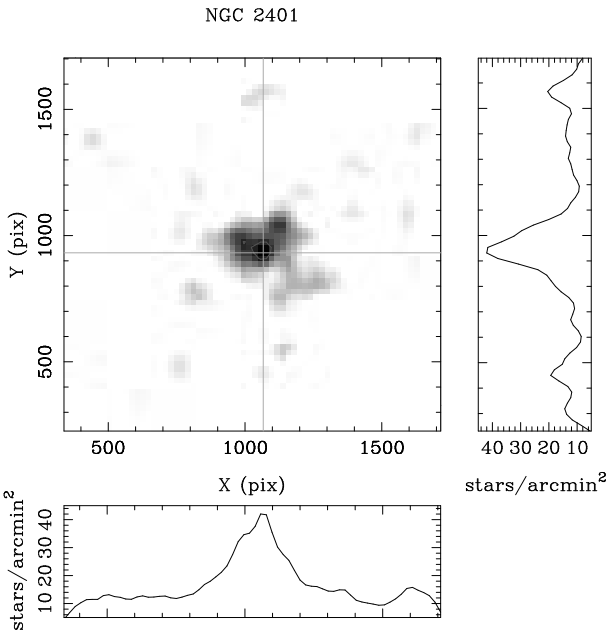

Figure 3. First approximation to the center determination for NGC 2401. Top Left: density map of the selected stars in the field. Top right: Y cut through the density maximum. Bottom: X cut through the density maximum.

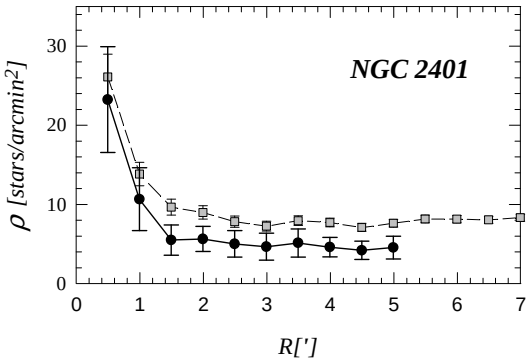

Figure 4. Radial density profiles for NGC 2401. Filled circles: CCD data. Grey squares: 2MASS data. Poisson error bars (1σ) are also shown.

3 ANALYSIS

3.1 Cluster center and size

As a first step, we estimated the position of the cluster center. This procedure was done by a combination of a visual inspection of the DSS-2 plates and the method given by Moitinho (1997). In this later case, the surface stellar distribution was convolved with a kernel and the center is adopted as the point of maximum density. In this case a 100×100 CTIO pixels ($\approx 0\farcm66\times0\farcm66$) gaussian kernel was used to smooth out the details of the spatial distribution and give a precise idea of the center position. Fig. 3 illustrates the method. The derived center was $\alpha_{2000}=07:29:25.2$; $\delta_{2000}=-13:57:54$, nearby to the one given by Dias et al. (2002) or by the $SIMBAD$ database.

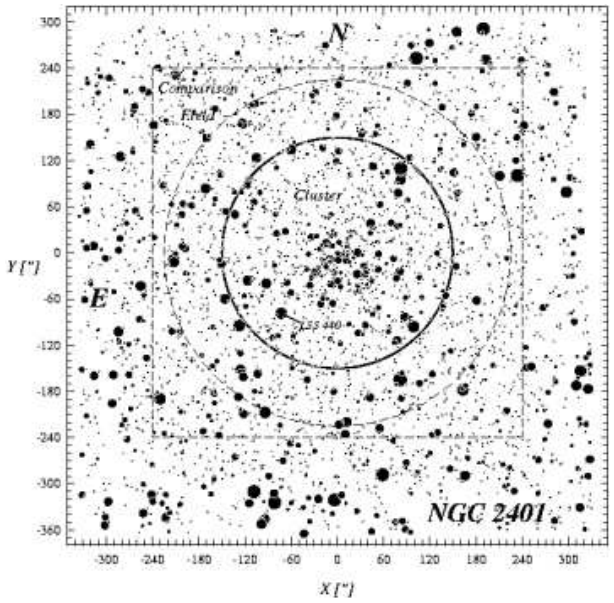

Figure 5. Finding chart of the observed region in NGC 2401 (V filter). The black solid circles, $2'.5$ in radius indicates the adopted angular size for the cluster (see Sect. 3.1 and Fig. 4). The short–dashed lines indicate the area adopted as a *Comparison Field* (CF). For a coordinate reference, the $X = 0$; $Y = 0$ values correspond to the cluster center coordinates $\alpha_{2000} = 07:29:25.2$; $\delta_{2000} = -13:57:54$ and all $X - Y$ are expressed in arcseconds.

The second step was to compute the cluster radial density profile by counting stars in a number of successive rings, $0'.5$ wide, and dividing the counts by the correspondent ring's area. We applied this method to both, the optical and the 2MASS infrared data. The respective radial density profiles are shown in Fig. 4. We appreciate a well shaped radial stellar density profile for the cluster with an important central concentration up to $\sim 1'.5$ but we adopted a radius of $R = 2'.5$ since at this value the stellar density reaches the (residual) field density. Our adopted value is a bit larger than the diameter of about $2'$ given by Lyngå (1987) and Dias et al. (2002). It seems that these works refer to the object size as only the very central part of the cluster. On the other hand, the radius we computed here is generous enough to include cluster stars (mainly faint ones) that could be placed a bit far from the cluster center. In any case, our data completely covers the cluster together with an important part of its surrounding field.

3.2 Optical data and cluster membership

Information about proper motions and radial velocities for the stars in the area of NGC 2401 is scarce. The UCAC2 catalogue (Zacharias et al. 2004) provides proper motion data for some stars in these area down to a magnitude about $V = 16$ that could help to perform a membership assignment. However, uncertainties of these measurements ($\sim 10\ mas/yr$) avoid using proper motions in a efficient way. Therefore, the only way to obtain a reliable membership assignment is by analyzing the individual position of the stars onto the several photometric diagrams (e.g. Baume et al. 2003, 2004).

The optical Two Color Diagrams (TCDs) and Color Magnitude Diagrams (CMDs) of NGC 2401 are shown in Figs. 6 and 7 respectively. The TCDs of Figs. 6, and the CMDs of Figs. 7ab and 7de include all the stars inside the adopted radius for the cluster (see Sect. 3.1). For reference purpose, we adopted a *Comparison Field* (CF) defined by the short–dashed lines in the finding chart of Fig. 5. This CF was chosen in such a way that its area equals the corresponding to the cluster and it was also totally covered by the NTT observations. The CMDs of the CF are shown in Figs. 7c and 7f.

Different CMDs show different limiting V magnitude going from ~ 19 in $U - B$ to ~ 23 in $V - I$ due to the not similar wavelength sensitivity of the detectors, on a side, and also because we combined data from two sources (see Sect. 2.1), on the other. Naturally, deep $V - I$ data came from the NTT.

All the diagrams confirm that NGC 2401 presents a very sharp, clear and blue main sequence (MS) above $V \sim 17 - 17.5$. For membership assignments, individual positions down to the magnitude limit were examined in all the photometric diagrams using the procedure described in Baume et al. (2004). This is:

- If stars brighter than $V \sim 16.5$ have coherent locations in all the TCDs and CMDs along the MS, they were adopted as likely members (lm). We shall discuss below the case of LSS 440 (see Sect. 4).
- Dimmer stars with magnitudes in the range $V \sim 16.5 - 17.5$ in the same conditions were considered only as probable members (pm).
- If some stars are brighter than $V \sim 16.5$, well placed onto the TCDs of Fig. 6 but located a bit over the ZAMS on Fig. 7, they were still considered as pm since their magnitude offsets could be due to a probable binarity effect. This was undoubtedly the case of stars # 66 and # 75 which, unlike likely members, appeared above the MS (~ 0.5 mag).
- Finally, the number of likely and probable member stars in each magnitude bin must keep a reasonable agreement with the counts that were obtained when CF stars were adequately subtracted from the $'cluster\ area'$ (see Sect. 5).

At fainter magnitudes, contamination by field stars becomes severe, preventing an easy identification of faint cluster members. Anyway, it was still possible to determine the number of probable faint cluster members in a statistical way (see Sect. 5 and Sect. 6).

3.3 Cluster parameters

3.3.1 Optical data

This region of the Third Galactic Quadrant is characterized by a reddening slope and a ratio of the total to selective absorption ($R = A_V/E_{B-V}$) that can be considered normal (Moitinho 2001). Since the picture presented in the $B - V$ vs. $V - I$ diagram in Fig. 6b agrees with this concept, we adopted standard ratios $E_{U-B}/E_{B-V} = 0.72 + 0.05\ E_{B-V}$ and $E_{V-I}/E_{B-V} = 1.244$ (Dean et al. 1978), which implies $R = 3.1$, to shift the Schmidt-Kaler (1982) ZAMS, the intrinsic lines from Cousins (1978ab) and the Girardi

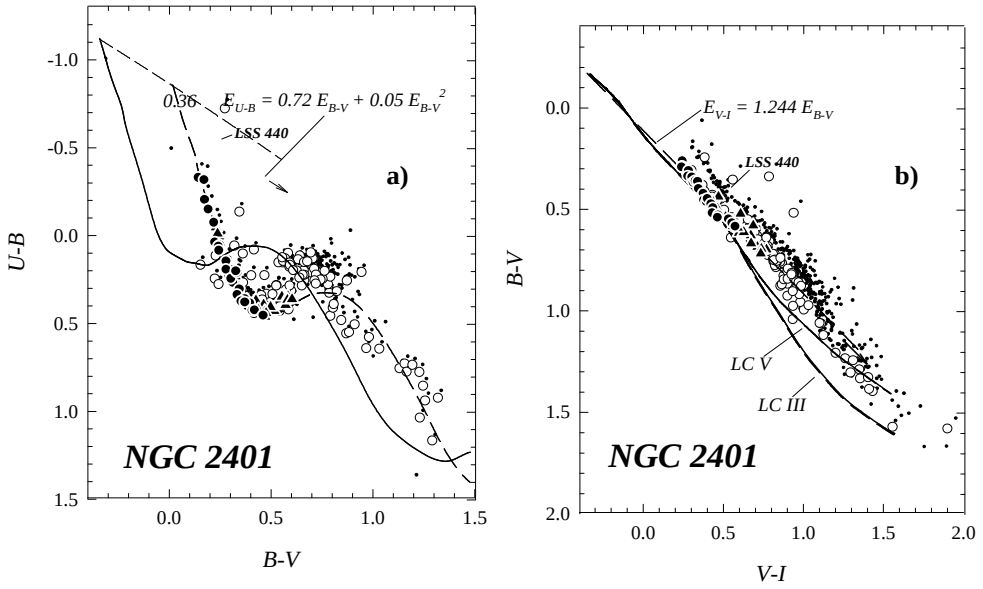

Figure 6. Optical TCDs of stars located inside the adopted radius of NGC 2401 **a)** $U-B$ vs. $B-V$ diagram. The symbols have the following meaning: black circles are adopted likely member stars (lm), black triangles are probable member stars (pm), white circles are non-member stars (nm), and dots are stars without any membership assignment. The solid line is the Schmidt-Kaler (1982) ZAMS, whereas the dashed one is the same ZAMS, but shifted by the adopted color excess (see Sect. 3.3). The dashed arrow indicates the normal reddening path. **b)** $B-V$ vs. $V-I$ diagram. Symbols and lines have the same meaning as in panel a).

et al. (2000) isochrones in the TCDs and CMDs. By restricting to lm and pm stars, we found mean excess values and standard deviations $E_{B-V} = 0.36 \pm 0.01$ and $E_{U-B} = 0.27 \pm 0.01$. As for the cluster distance modulus we found $V - M_V = 15.1 \pm 0.2$ (error from eye-inspection) by the fitting method. This distance modulus combined with a mean visual absorption $A_V = 1.12$ places NGC 2401 at 6.3 ± 0.5 kpc from the Sun.

The age of the cluster was derived superposing the isochrones of Girardi et al. (2000), computed with mass loss and overshooting (see Fig. 10) and solar metallicity, and looking for those ones that produce the best fit over the stars along the upper MS. This method yields that NGC 2401 is about 20 ± 5 Myr old. Another age indicator comes from the inferred earliest spectral type at the upper MS of the cluster. In NGC 2401, the earliest MS star may have a spectral type B3 and, according to the calibration given by Meynet et al. (1993), the corresponding age is about 30 Myr. We adopted then 25 ± 5 Myr as a good estimation for NGC 2401 age.

3.3.2 Infrared data

As a control of the optical findings, we built up the CMDs indicated in Fig. 8 using 2MASS data (see Sect. 2.3). If we only consider the infrared colors (Fig. 8a), the data spread of lm and pm stars is very significant though their mean values approximately follow the MS position given by Koornneef (1983). It is obvious that this spread is due to the infrared magnitude errors in the 2MASS catalogue at the level of $K \approx 14 - 15$ as it is strongly reduced when combined with optical data to obtain the $V - K$ index (Fig. 8b). So, the distance modulus fit in the infrared diagrams turns out to be quite acceptable; in addition, infrared diagrams independently confirm that the reddening law is normal as suggested by the optical TCDs of Fig. 6.

As a final note, the infrared CMD of the CF (see Sect. 3.2) which is shown in Fig. 8c confirms that the region around the MS has almost no stars reinforcing the real nature of the cluster.

4 THE BE-TYPE STAR LSS 440

A singular object in the field of NGC 2401 is the bright star # 14 located at 1′.8 south-east from the cluster center. This star was early identified by Stephenson & Sanduleak (1971) as LSS 440 who informed it is an OB-type star with the Balmer continuum in emission (in an exceptionally pronounced way) and the H_α line in emission too according to an independent H_α plate. To classify this star a series of spectra were obtained covering the spectral range 3400 Å - 6750 Å(see Sect. 2.2). The LSS 440 spectrum is shown in Fig. 9 together with a detail of the most relevant features. This star shows the H_α line in strong emission, together with H_β and H_γ lines in clear core emission and H_δ only in a weak way. The FeII 27, 37, 38, 42, 48, 49 and SiI 19, 26 multiplets also appear in emission. The Balmer continuum is in emission too, but not as strong as Stephenson & Sanduleak (1971) claimed. The H_α equivalent width is $\sim$ 76 Å and the rotation velocity is near $v\ sin\ i \sim 270 - 300$ km/sec from HeI lines 4471 and 4026.

The spectral classification of LSS 440 was performed using the BCD spectrophotometric system (see Barbier & Chalonge 1941, Chalonge & Divan 1952, 1973 and Cidale et al. 2001 for the description of the method). Briefly, the method is based on the study of the Balmer discontinuity, which is independent on interstellar and circumstellar extinctions. Using then the obtained BCD parameters $\lambda_1 = 59.7$ Å, $D = 0.078$ dex and calibration tables given by Zorec (1986), we classified this star as B0 Ve. The early type and the

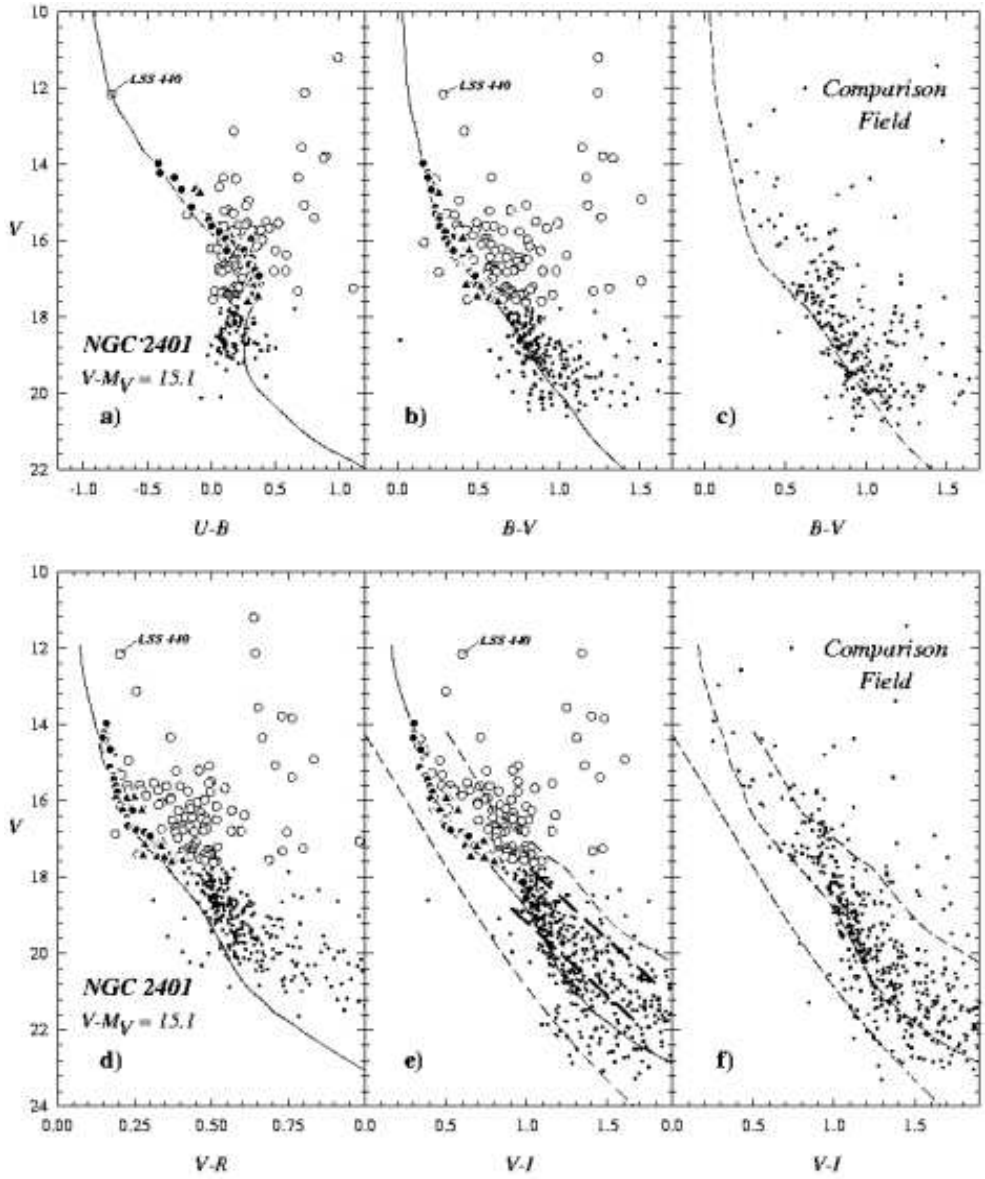

Figure 7. Optical CMDs of stars located inside the adopted radius of NGC 2401 ($'cluster\ area'$, panels a, b, d and e) and in the adopted CF (panels c and f). Symbols have the same meaning as in Fig. 6. The solid lines are the Schmidt-Kaler (1982) and Cousins (1978ab) empirical ZAMS and MS respectively, corrected for the effects of reddening and distance. The adopted apparent distance modulus is $V - M_V = 15.1$ ($V - M_V = V_0 - M_V + 3.1E_{B-V}$, see Sect. 3.3). Dashed lines showed on the CF diagrams have the same meaning as the curves in the other panels: ZAMS, MS and the adopted envelopes used to compute the LF (see Sect. 5). See Sect. 6 for the meaning of long dashed right lines on panel e)

presence of emission FeII lines could indicate LSS 440 as a member of Group I according to the classification scheme proposed by Jaschek et al. (1980).

The models given by Zorec et al. (2002) can be used to get the average photospheric properties for this star as well: $M_V = -3.6 \pm 0.5$; $T_{eff} = 30000 \pm 1000\ K$; $log\ g = 4.0 \pm 0.1$ and $M_{bol} = -6.5 \pm 0.2$. Combining with Girardi et al. (2000) evolutionary models of solar metallicity, a star with such properties should have a mass near 15 $\mathcal{M}_\odot$ and an age about 5-6 10^6 yr.

Likewise, based on the slope change of the star spectra from 4000 Å to 4600 Å , and using the Chalonge & Divan (1973) calibration improvements to the BCD method by Cidale et al. (2001), we can compute the star visual absorption (A_V) produced by both the interstellar dust and the circumstellar envelope. The computations yielded $A_V = 1.33$ setting the true distance modulus of LSS 440 in $V_O - M_V = 14.44 \pm 0.5$ corresponding to a distance $d = 7.7$ kpc.

Fabregat & Torrejon (2000) studied the abundance of Be stars in open clusters as a function of the cluster ages. Following these authors findings Be-type stars show a maximum of appearance in clusters the age of NGC 2401. From this point of view, to find a Be-type star in this cluster should not be odd. However, the distance of LSS 440 disagrees with the cluster distance and it is placed a bit far from the clus-

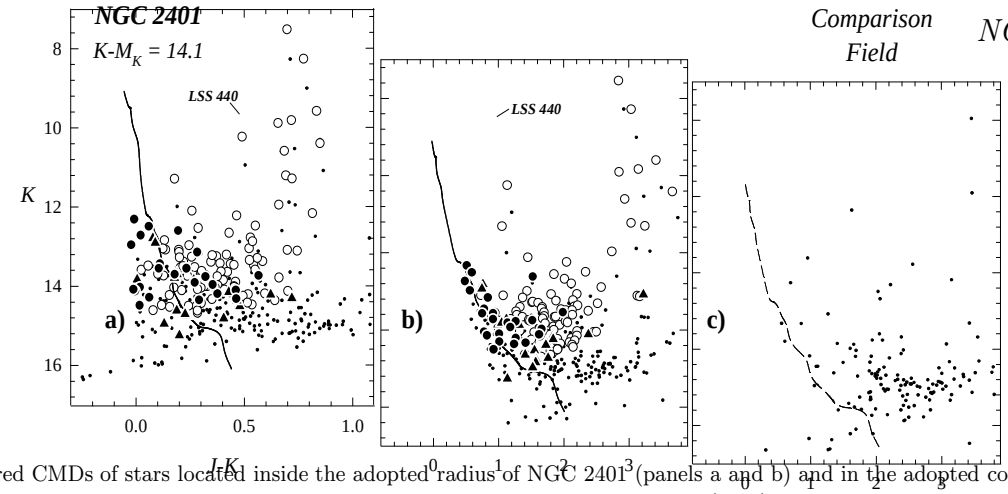

Figure 8. Infrared CMDs of stars located inside the adopted radius of NGC 2401 (panels a and b) and in the adopted comparison field (panel c). Symbols have the same meaning as in Fig. 6. The solid lines are the Koornneef (1983) empirical MS, corrected for the effects of reddening and distance ($K - M_K = 14.1 = V_0 - M_V + (3.1 - 2.78)\ E_{B-V}$, see Sect. 3.3). Dashed line showed on the comparison field has the same meaning as the curves in the other panels.

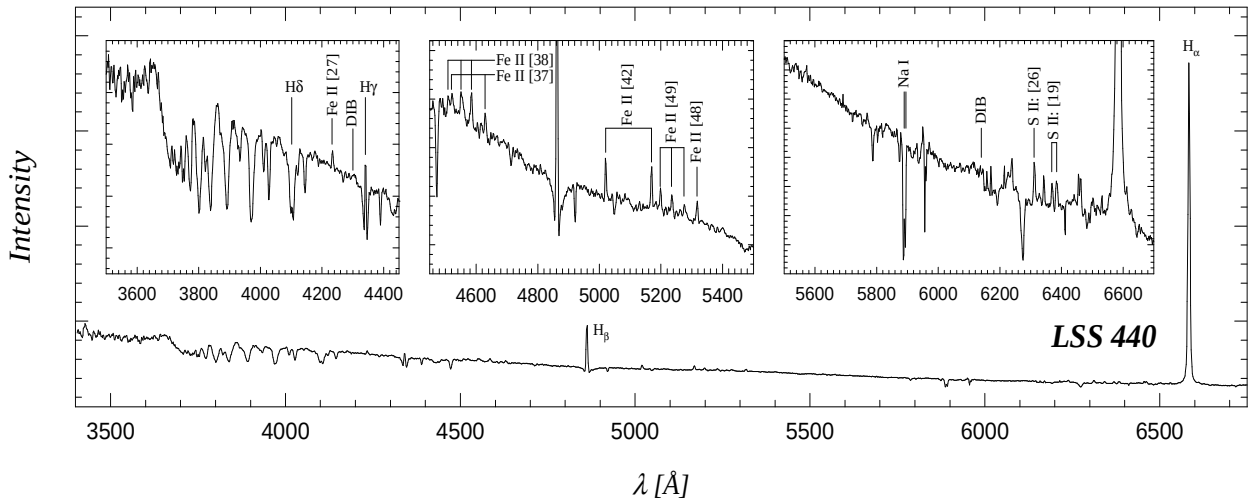

Figure 9. Complete observed spectrum of LSS 440 star on the main panel and its main features in detail on the three upper minor panels

ter center. Likewise, the mass of LSS 440 is extremely high if compared to the mass of next bright member star onto the cluster MS (see Sect. 3.3 and Sect. 5 in advance) which is $\approx 2mag$ fainter. Certainly, the location of LSS 440 onto the M_V vs. $B-V$ and $U-B$ vs. $B-V$ diagrams are in agreement with the usual location of other Be stars in open clusters (see Figs. 6a and 7 given by Mermilliod 1982) but the available elements at the moment preclude any kind of clear physical relationship between the cluster and this star. Radial velocities would be a very useful tool to settle this question.

5 CLUSTER LUMINOSITY AND INITIAL MASS FUNCTIONS

For the construction of the cluster luminosity function, defined as the distribution of stars over the magnitude range in bins 1^m wide, we applied the procedure already described in Baume et al. (2004). That is, we first computed the apparent magnitude distribution of lm and pm stars for $V < 17$ (LSS 440 star was not included in this analysis) and from the substraction method for $V \geq 17$.

The latter procedure consists in a "cleaning" of the CMD of all stars inside the cluster limits by removing the contribution of field stars projected onto the cluster itself. We assume that our CF provides a good estimation of the contamination by field interlopers and is valid across the $'cluster\ area'$. We tried to reduce the contamination coming from the Galactic disk population by means of two envelope curves around the MS on the V vs. $V-I$ plane (dashed curves on Figs. 7ef). We located them reasonably far from the MS in order to include all cluster stars. Then we used a separation from the MS of about 0.3^m in color for a given V magnitude, a value that was increased to faint magnitudes according to photometric errors. It is to be mentioned that the completeness of our data has been estimated as in Baume et al. (2004) and like in that case incompleteness is only severe at very faint magnitudes ($V > 21$).

Once the entire distribution of apparent magnitudes is

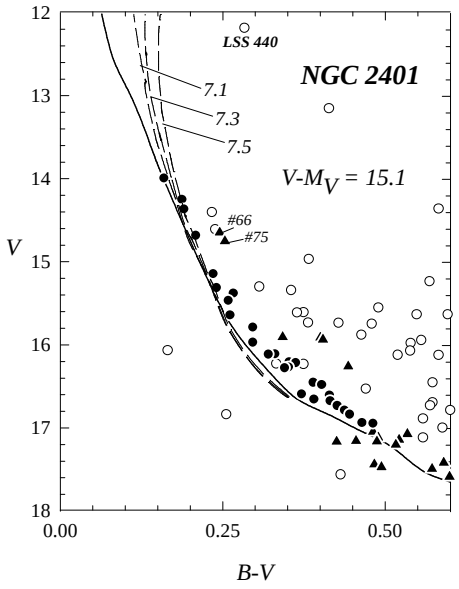

Figure 10. V vs. $B-V$ CMD showing the isochrones (dashed lines) from Girardi et al. (2000) and the Schmidt-Kaler (1982) ZAMS (solid line) corrected for the effects of reddening and distance (see Sect. 3.3). Symbols have the same meaning as in Fig. 6. The numbers indicate log(age).

Table 2. Stellar counts, completeness values and apparent cluster LF

Δ V	Cluster Area	Comparison Field	Completeness [%]	Apparent LF
14-15	8	2	100.0	6
15-16	20	7	100.0	10
16-17	38	11	99.8	18
17-18	55	42	97.3	15
18-19	94	59	96.2	36
19-20	106	69	95.5	39
20-21	99	85	94.2	15
21-22	110	98	91.8	13
22-23	125	99	78.4	33
23-24	46	19	57.3	47

ready, it is transformed into the M_V distribution using the cluster distance modulus of Sect. 3.3. The results are presented in Table 2 in a self explanatory format.

Regarding the IMF, which is defined as the distribution of original ZAMS stellar masses in logarithmic bins, absolute magnitude intervals of the LF were converted into mass intervals using the mass-luminosity relation given by Scalo (1986). What we obtained is indeed the Present Day Mass Function (PDMF) which in the case of NGC 2401 is very close to the IMF because only stars below the "turn-off" are considered. The results shown in Fig. 11 indicate that the IMF displays a constant slope for the most massive bins (filled circles) while a small dip appears at about 2 $M_\odot$ followed by another one, more noticeable, near 0.8 $M_\odot$. Since the last (less massive) mass-points (open circles) are dubious because of probable incompleteness, the dip could be an artifact; if not, they are suggesting a pronounced flat-

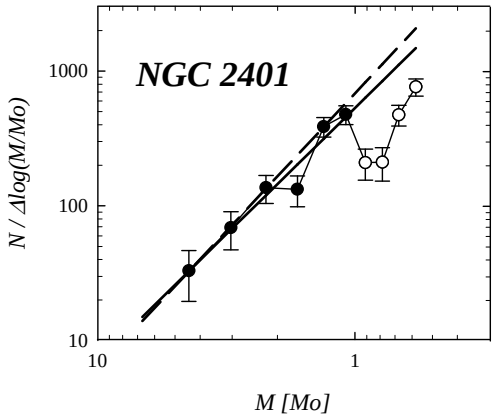

Figure 11. Initial Mass Function (IMF) of NGC 2401. Error bars are from Poisson statistics. The weighted least square fittings for the more massive bins are indicated by solid and dashed right lines (open symbols indicate bins not used in the fits. See Sect. 5 for details).

tening of the mass function. The mass-points of the most massive stars were fitted through a weighted least squares fit that yielded a slope $x = 2.0 \pm 0.1$ for $M > 2$ $M_\odot$ and $x = 1.8 \pm 0.2$ for $M > 1$ $M_\odot$ (see Fig. 11).

6 A PROBABLE PMS STAR POPULATION IN NGC 2401

No doubt NGC 2401 is young and could still show hints of a PMS star population which is normally placed over the fainter part of the cluster above the MS. In fact, Figs. 7de suggest the presence of a "turn–on" point at $V \sim 17-18$; however the detection of a PMS star population at this magnitude level is hard due to the field contamination. Figs. 7ab, on the other hand, are not deep enough to perform a trustable analysis of this type.

In order to clarify this point, we applied again the substraction procedure using Figs. 7ef (see Sect. 5), but now selecting also stars by $V-I$ bins 0.25^m wide (see Baume et al. 2003). This way we could build an array indicating the amount of stars in each V and $V-I$ box, both for the $'cluster\ area'$ and for the CF. By performing then the difference between these two arrays, we notice an excess of stars present approximately in the path indicated by the long dashed right lines on Fig. 7e. This fact reinforces therefore the probable existence of a PMS star population in NGC 2401. However, deeper photometric observations and/or spectroscopy of selected stars in this region would be important to confirm this issue.

7 NGC 2401 AND THE GALACTIC STRUCTURE IN THE THIRD GALACTIC QUADRANT

The distance and age of NGC 2401 (see Sect. 3.3) indicate this object belongs to the innermost side young population of the probable extension of the Norma-Cygnus spiral–arm in the Third Galactic Quadrant. This outer spiral structure was already suggested by Vogt (1976) using Luminous Stars

and, more recently, by Kaltcheva & Hildilch (2000) studying OB stars. Star forming regions were found by Russeil (2003), though an inspection of his Fig. 5 shows few young objects at the galactic position of NGC 2401. The Georgelin & Georgelin (1976) list shows just one Hα source, S 298, at a distance of 5.2 kpc but with a galactic longitude of 227.7°. Also, few open clusters with ages less than 100 Myr are found in this region when inspecting the Dias et al. (2002) catalogue. It is obvious that the Norma-Cygnus arm can be optically detectable partially through windows in the interstellar absorption. However, May et al. (2005) could trace this spiral–arm by means of CO clouds and optical evidences of its existence have also been recently reported by Carraro et al. (2005b) who detected the presence of a large population of blue distant stars behind several open clusters in this Galactic Quadrant. In this sense, the cluster upper MS (see Fig. 7) of NGC 2401 coincides with the 'blue plume' seen in the cluster sample analyzed by Carraro et al. (2005b) which they associate to a young population defining the Norma-Cygnus spiral–arm. In fact, the brightest stars of NGC 2401 appear at $V \approx 14-15$ and $B-V \approx 0.1$ and merge with old disc population at $V \approx 18$ just as stars in the 'blue plume' of Carraro et al. (2005b) do. So, NGC 2401 is then part of the small sample of very young open clusters presently known to trace the Norma-Cygnus arm: Bochum 2, Haffner 18, Dolidze 25 and Pismis 1, among others. The spatial distribution of CO clouds (May et al. 2005), the young distant population (Carraro et al. 2005b) and the distance of NGC 2401 suggest altogether it is located in the innermost side of the Norma-Cygnus arm. Therefore, NGC 2401 CMDs can be used in the future as a possible template to recognize and match features such as the mentioned 'blue plume' seen in the optical CMDs of other places in the Third Galactic Quadrant.

We also have shown arguments that weaken the probable relationship of LSS 440 to NGC 2401: LSS 440 is placed at a distance $d = 7.7$ kpc, but the error in its M_V estimate and in the cluster distance modulus may locate the star as far from the Sun as 9.5 kpc or as close to it as 6.1 kpc. Only in this late marginal case, some relation can be stated, but we have already shown other arguments such as the star mass against that. By ignoring any connection between the cluster and the star, it becomes evident that unlike NGC 2401, LSS 440 is located well inside the Norma-Cygnus spiral–arm so that, in any case, we are dealing with very young and remote objects that reinforce the spiral structure of the Milky Way in this quadrant of the Galaxy.

8 CONCLUSIONS

We have presented a detailed multicolor photometric study in the region of the open cluster NGC 2401, we confirmed the emission nature of LSS 440 and gave its first spectral type classification. In our opinion, the present state of knowledge of this star precludes discard its membership to the cluster but no firm argument favoring its cluster membership has been found. NGC 2401 is a very young object (~ 25 Myr) placed at 6.3 ± 0.5 kpc from the Sun what makes it an object located in the outskirts of our galaxy and therefore a good tracer of the continuation of the Norma-Cygnus arm into the Third Galactic Quadrant. Not confirmed at all, we found weak evidences of a probable PMS star population accompanying this cluster. As for the cluster IMF, the slope value found for NGC 2401 is not far from the typical values shown by Scalo (1998, 2005).

ACKNOWLEDGEMENTS

The authors thank the CASLEO staff for the technical support and the very useful discussions and valuable comments from L. Cidale. AM thanks the financial support from FCT (Portugal) grants BPD/20193/99, SFRH/BPD/19105/2004 and the YALO project (PESO/P/PRO/1128/96). GB acknowledges a postdoctoral grant from Padova University where part of this work has been made. GC work has been partially supported by *Fundación Andes*. This research has been also carried out under the cooperative international agreement Argentino-Italiano SECYT-MAE (IT/PA03 - UIII/077). We are much obliged for the use of the NASA Astrophysics Data System, of the Simbad database (Centre de Donnés Stellaires — Strasbourg, France) and of the WEBDA open cluster database. This publication also made use of data from the Two Micron All Sky Survey, which is a joint project of the University of Massachusetts and the Infrared Processing and Analysis Center/California Institute of Technology, funded by the National Aeronautics and Space Administration and the National Science Foundation.

REFERENCES

Barbier D. & Chalonge D. 1941 Ann.Astrophys. 4, 30
Baume G., Vázquez R.A., Carraro G. & Feinstein A. 2003, A&A 402, 549
Baume G., Moitinho A., Giorgi E.E., Carraro G. & Vázquez R.A. 2004, A&A 417, 961
Chalonge D. & Divan L. 1952, Ann.Astrophys 15, 201
Chalonge D. & Divan L. 1973, A&A 23, 69
Carraro G. & Munari U. 2004, MNRAS 347, 625
Carraro G., Geisler D., Baume G., Vázquez R.A. & Moitinho A. 2005a, MNRAS 360, 655
Carraro G., Vázquez R.A., Moitinho A. & Baume G. 2005b, ApJ 630, L153
Cidale L., Zorec J. & Tringaniello L. 2001 A&A 368, 160
Cousins A.W.J. 1978a, MNSSA 37, 62
Cousins A.W.J. 1978b, MNSSA 37, 77
Dean J.F., Warren P.R. & Cousins A.W.J. 1978, MNRAS 183, 569
Dias W.S., Alessi B.S., Moitinho A., et. al 2002, A&A 389, 871
Fabregat J. & Torrejón J.M. 2000, A&A 357, 451
Georgelin Y.M. & Georgelin Y.P. 1976 A&A 49, 57
Giorgi E.E., Vázquez R.A., Baume G., Seggewiss W. & Will J.-M. 2002, A&A 381, 884
Giorgi E.E., Baume G., Solivella S. & Vázquez R.A. 2005, A&A 432, 491
Girardi L., Bressan A., Bertelli G., & Chiosi C. 2000, A&AS 141, 371
Høg E., Fabricius C., Makarov V.V. et al. 2000, A&A 357, 367
Jaschek M., Jaschek C., Hubert-Delplace A.-M. & Hubert H. 1980, A&AS 42, 103
Kaltcheva N.T. & Hildilch R.W. 2000, MNRAS 312, 753
Koornneef J. 1983, A&A 128, 84
Lyngå G. 1987, Catalog of Open Star Cluster Data, Strasbourg, CDS

Martin N.F., Ibata R.A., Bellazzini M. et al. 2004, MNRAS 348, 12
May J., Alvarez H. & Bronfman L. 2005, submitted
Mermilliod J.-C. 1982, A&A 109, 48
Meynet G., Mermilliod J.-C & Maeder, A. 1993, A&AS 98, 477
Moitinho A., Alfaro E.J., Yun J.L., & Phelps R.L. 1997, AJ 113, 1359
Moitinho A. 2001, A&A 370, 436
Moitinho A. 2002, in Modes of Star Formation and the Origin of Field Populations, ASP Conference Proceedings, Vol. 285. Edited by Eva K. Grebel and Walfgang Brandner. San Francisco: Astronomical Society of the Pacific, 2002., p.256
Moitinho A., Carraro G., Baume G. & Vzquez R.A. 2005, A&A (accepted)
Momany Y., Zaggia S.R. Bonifacio P. et al. 2004 A&A 421, L29
Russeil D. 2003 A&A 397, 133
Scalo J. 1986, Fund. Cos. Phys. 11, 1
Scalo J. 2005, in IMF@50: The Initial Mass Function 50 Years Later, ed. E. Corbelli, F. Palla, & H. Zinnecker (Dordrecht: Kluwer), in press (astro-ph/0412543)
Schmidt-Kaler Th. 1982, Landolt-Börnstein, Numerical data and Functional Relationships in Science and Technology, New Series, Group VI, Vol. 2(b), K. Schaifers and H.H. Voigt Eds., Springer Verlag, Berlin, p.14
Stephenson C.B. & Sanduleak N. 1971, Publ. Warner & Swasey Obs. 1
Sujatha S., Babu G.S.D. & Ananthamurphy S. 2004, Bull. Astr. Soc. India 32, 295
Vogt N. 1976, A&A 53, 9
Zacharias N., Urban S.E., Zacharias M.I. et al. 2004, AJ 127, 3043
Zorec J. 1986, in *Thèse d'État*, Université Paris VII
Zorec J, Fre'mat Y, Huber A.M. & Floquet M. 2002, in ASP Conf.Ser.259: IAU Colloq.185: Radial and non-radial Pulsations as Probes of Stellar Physics, 244